1. interaction mechanisms with satellites and Io's torus; these mechanisms must account for the characteristics of the Io absorption features as a function of particle species and energy;
2. acceleration of electrons and protons in the middle and outer magnetospheres, both time averaged and on a timescale of a few minutes;
3. the structure and motion of the plasma disc in the middle magnetosphere;
4. access of ions from the Io torus and interplanetary space into the outer magnetosphere and their subsequent acceleration;
5. the clock modulation of energetic electron fluxes in the outer magnetosphere and in the interplanetary medium; and
6. the mechanism for releasing energetic electrons into interplanetary space and modulating this release with the Jovian rotation period.

Answers to these questions will require a better definition of the properties of the energetic-particle population. Some of this information will emerge from further evaluation of Voyager and Pioneer data; however, new observations with more sophisticated instruments are needed. Crucially important are a greater local-time coverage, a larger time base to distinguish spatial from temporal variations, an extended coverage of lower-energy particles, and an extension of the frequency range of wave measurements.

6

SPECTROPHOTOMETRIC STUDIES OF THE IO TORUS

Robert A. Brown, Carl B. Pilcher, and Darrell F. Strobel

6.1. Introduction

A toroidal volume near Io's orbit is made luminous by multiple optical and ultraviolet line emissions excited by resonant scattering of sunlight and by electron collisions. These emitting atoms and ions have been lost from Io. Table 6.1 summarizes the species and detected transitions as of early 1982. In this chapter we focus on spectrophotometric measurements of these emissions and their physical interpretation. The reader is referred to Pilcher and Strobel [1982] for a more general view of torus emission phenomenology.

The concept of circumplanetary atoms of satellite origin was first proposed by McDonough and Brice [1973] for Titan, a satellite with a dense atmosphere from which Jeans escape is probably important. The Io phenomenon was not anticipated owing to Io's low atmospheric pressure [Smith and Smith, 1972; Pearl et al., 1979]; nevertheless, the discovery by R. A. Brown [1974] of sodium optical emission from Io's vicinity established the first example of a satellite that is a rich, continuing source of material for a planetary environment. We know now that the flow of material from Io dominates the particle and energy budgets of the Jovian magnetosphere.

The primary spatial reference here is to a toroidal volume of $\sim 4 \times 10^{31}$ cm^3 between about 5 and 7 R_J from Jupiter, which includes Io's orbit but lies near the magnetic equatorial plane or centrifugal symmetry surface. This torus contains the bulk of Io's neutral atom clouds and coincides roughly with the UV source region seen by Voyager.

We refer here approximately to the Voyager epoch, the period of the most comprehensive observations. There is intriguing but sometimes conflicting evidence about the plasmasphere's long-term stability, which casts a shadow across the deductions that follow. Spatial inhomogeneity and short-term variability undoubtedly exist. Our simplified picture, based on average properties, is inadequate for such detail and presents some danger of missing a fundamental point associated with, say, nonlinearity or disequilibrium. Nevertheless, we are led by many lines of inference to well-delineated spatial, energetic, and compositional regimes for Jupiter's thermal plasma.

Eight years of study of the manifold emission phenomena associated with the Io torus have produced two kinds of results: (1) demonstrations that certain physical processes obtain in the torus and (2) inferences about the composition and physical state of the torus based on theoretical understanding of the various mechanisms of light production. It is our purpose in this chapter to review these observations, their rationale and implications, plus their relationship to in situ studies of the Jovian environment by the Pioneer and Voyager spacecraft.

6.2. Observational basis: apparent emission rates

This section states the geometrical relationship between the emission and the remote observation of light, incidentally defining the Rayleigh, the photometric unit for

Table 6.1. *Observed emitting species in the Io torus*

Species[a]	Source of detection[b]	Excitation mode[c]	Transition type
Na I	GB	RS	Allowed
K I	GB	RS	Allowed
S II	IUE	Coll	Allowed
	Voyager	Coll	Allowed
	GB	Coll	Forbidden
S III	Voyager	Coll	Allowed
	IUE	Coll	Allowed
	GB	Coll	Forbidden
S IV	Voyager	Coll	Allowed
O I	GB	Coll	Forbidden
O II	Voyager	Coll	Allowed
	GB	Coll	Forbidden
O III	Voyager	Coll	Allowed
	IUE[d]	Coll	Allowed
	(GB)[e]	Coll	Forbidden

[a] I indicates the neutral, II indicates single ionization, III indicates double ionization, and so forth.
[b] GB = Ground-based; IUE = international ultraviolet explorer.
[c] RS = resonant scattering; Coll = collisional excitation.
[d] Marginal detection by Moos and Clarke (1981).
[e] Stringent upper limit to [O III] 5007A emission by Brown, Shemansky, and Johnson (1982).

expressing the brightness of line emission [Chamberlain, 1961]. This formalism is the context for decoding the light received from the Io torus in terms of underlying physical and compositional parameters.

Figure 6.1 depicts a telescope having collecting area $A(\text{cm}^2)$ and field of view Ω (sr) observing an emitting layer that is differentially thin and oriented perpendicular to the line of sight. The surface brightness is dJ_λ (photons/cm^2/sr/s) owing to light emission at nominal wavelength λ by particles in the layer. The photon count rate (for unit instrumental efficiency) is

$$\text{count rate } (\text{s}^{-1}) = dJ_\lambda A\,\Omega = dJ_\lambda A\,\frac{a}{r^2} \tag{6.1}$$

In the differential volume, adr, the number density of emitter is n (cm^{-3}) and the average number of photons emitted in the line by each atom or ion per second is ϵ_λ, the unit emission rate. If the emission is isotropic, the photon count rate at the telescope is

$$\text{count rate } (\text{s}^{-1}) = nadr\epsilon_\lambda\,\frac{A}{4\pi r^2}$$

which in combination with (6.1) yields:

$$4\pi dJ_\lambda = n\epsilon_\lambda dr$$

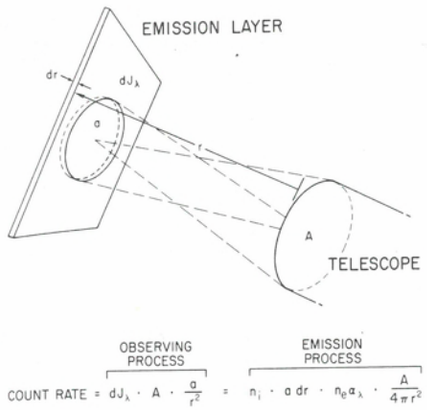

Fig. 6.1. The geometry for remote observations of emitting regions. The count rate for photons at the telescope is computed from two perspectives to derive the result (6.2) relating the observed brightness to the physical process of emission along the line of sight.

By integrating along the line of sight through the source region, we obtain

$$4\pi J_\lambda = \int n(r)\epsilon_\lambda(r)dr \tag{6.2}$$

The left side of (6.2) is the observed quantity, known as "the apparent emission rate"; if J_λ is expressed in units of 10^6 photon/cm^2/sr/s, then $4\pi J_\lambda$ is in Rayleighs.

The right side of (6.2) is the sum along the line of sight of the number density of emitters weighted by their propensity to emit. The density factor reflects composition; the unit emission rate factor responds to the radiation or charged particle environment of the atoms or ions. When observations are interpreted, this reciprocity in the density-emission rate product causes an ambiguity between composition and physical conditions that can be resolved only by means of external information or assumptions.

In the case of the alkali metal atoms in the Io torus, sunlight is resonantly scattered (absorbed and reemitted) in permitted atomic transitions such as the sodium *D*-lines; ϵ_λ is proportional to the solar flux at λ and the atomic oscillator strength. For sulfur and oxygen atoms and ions, electrons populate upper atomic levels by means of inelastic collisions, and the atom or ion decays to the ground state by the emission of one or more photons. In this case, ϵ_λ is the product of the electron number density n_e and a rate coefficient $\alpha_\lambda(T_e, n_e)$ which is a function not only of electron temperature but also of electron number density, owing to collisional deexcitation.

When little supporting information is available about the variations of $n(r)$ and $\epsilon_\lambda(r)$ along the line of sight, it is customary to simplify (6.2) to derive the average or characteristic parameters implied by an observations. If the excitation mechanism is known and can be assumed invariant along the line of sight, then the column abundance of the emitting species is

$$N \equiv \int n(r)dr = \frac{4\pi J_\lambda}{\epsilon_\lambda}\ (\text{cm}^{-2}) \tag{6.3}$$

This expression is the basis, for example, of neutral sodium atom inventories around Io. For an assumed lifetime against loss, that inventory yields an estimate of the sodium production rate. Calculations of this nature are discussed in Section 6.3.

If the depth (D) of the emitting region can be estimated and uniform number density and excitation conditions are assumed, a useful form of (6.2) is

$$\overline{n\epsilon_\lambda} = \frac{4\pi J_\lambda}{D}\ (\text{photons/cm}^3/\text{s}) \tag{6.4}$$

This expression is the basis for estimates of the plasma energy loss rate per unit volume through collisionally excited emissions. If the electron number density and temperature can be estimated, then (6.4) yields the average or characteristic atomic or ionic number density.

$$\bar{n} = \frac{4\pi J_\lambda}{n_e \alpha_\lambda(T_e, n_e) D} \tag{6.5}$$

For two collisionally excited lines originating with the same emitting species, the apparent emission rate ratio,

$$\frac{4\pi J_{\lambda 1}}{4\pi J_{\lambda 2}} = \frac{\overline{\alpha_{\lambda 1}(T_e, n_e)}}{\overline{\alpha_{\lambda 2}(T_e, n_e)}} \tag{6.6}$$

is a diagnostic indicator of electron temperature or number density or a combination of the two. Two lines in the same multiplet may have closely spaced upper levels that are excited in a constant ratio independent of electron temperature. Collisional deexcitation from these levels competes increasingly with radiative decay as the electron number density increases. Because the excited levels have different lifetimes, this effect becomes important for one level before the other, and the ratio of the two emissions is a function of n_e in that transition range of electron density. When two lines originate in different multiplets, that is, from upper levels belonging to different terms, the emission ratio is a function of the electron temperature. The upper levels are excited in proportion to the fraction of electrons with greater than threshold energy, which is different for the two terms.

The red doublet of singlet ionized sulfur (6716 A, 6731 A) is an example of a case with α_N effectively temperature independent [Brown, 1976], permitting the electron density to be determined from the line ratio. The rate coefficients for 1304 and 6300 A emission from neutral oxygen and 685 and 6312 A emission from doubly ionized sulfur are effectively independent of electron number density under Io torus conditions [Brown, 1981a]; both line ratios yield direct estimates of electron temperature.

Equation (6.2) and its daughter expressions are powerful and convenient tools for inverting photometric observations of line emission in terms of the underlying composition and physical state. However, the observed volume is vast, complex, and detailed; assumptions of uniformity are generally false. Derived results are not literal, they are indicative. They join with other observations and inferences to improve our understanding of the Io torus.

6.3. The atomic clouds

Na *D*-line optical emission (5890 A, 5896 A) from the near-Io cloud is a bright, accessible phenomenon, and faint *D*-line emission is observed throughout the Jupiter magnetosphere. The near-Io cloud and one form of remote sodium appear to be kinematically related, while a second remote form requires an episodic acceleration mechanism [Brown and Schneider, 1981]. A sodium source at Io of $\sim 10^{27}$ atoms/s is required to sustain this tableau. Sodium is the best studied atomic species and serves as an archetype for our discussion of the neutral clouds.

Neutral cloud investigations have been of two types: (1) column abundance determinations in which (6.3) is used to invert brightness measurements, and (2)

kinematic studies in which measurements of Doppler shifts are used to determine line-of-sight velocities. We present the historical interpretation of these observations, but we caution the reader of a general failure to account adequately for modification of the observed morphological and kinematic structures by ionization and collisions. Although those processes have demonstrated importance for sodium cloud analysis, they have not been incorporated into superseding models. In following a chronological line with simplified but outdated conclusions, we mean to preserve the overall intellectual fabric while exposing the points ready for patches or replacement.

In simple form, the story told by the Na *D*-line observations is that of vast numbers of atoms traversing ballistic trajectories threading the entire Jovian magnetosphere. If the atomic lifetime is spatially invariant, the spatial distribution of these atoms is isomorphic to the source of same-element ions, because each atom may be ionized at a random time and place in its orbit. Before the discovery of an extended neutral oxygen cloud [Brown, 1981a], it seemed that the distribution of alkali metal atoms might be fundamentally different from that of the dominant plasma consituents, sulfur and oxygen probably originating in Io's sulfur dioxide atmosphere. Brown and Ip [1981] have argued that all heavy elements in the Jovian magnetosphere may arise and disperse from Io in a similar fashion. This neutral-phase generation has important implications for the energetics and spatial distribution of the thermal plasma.

Morphology and kinematics

Following the initial demonstration that *D*-line radiation emanates from a substantial volume of space surrounding Io [Trafton et al., 1974; Mekler and Eviatar, 1974], it was shown that the brightness of the sodium near Io varies sinusoidally with Io's orbital longitude, exhibiting a maximum when Io is at elongation [Bergstralh et al., 1975, 1977; see also Macy and Trafton, 1975a,b]. This is the signature of excitation by resonant scattering of sunlight. The modulation is caused by the oscillating heliocentric Doppler shift, which causes the Io sodium atoms to sample the deep Fraunhofer *D* lines at varying height.

Images of the near-Io sodium cloud [Matson et al., 1978; Murcray and Goody, 1978] led to the conclusion that sodium atoms escape Io with a residual velocity of a few km/s [Matson et al., 1978; Smyth and McElroy, 1978]. It was inferred from the asymmetric spatial distribution of this cloud that atoms originate from an extensive portion of the satellite near the sub-Jupiter point. In their imaging study, Murcray and Goody [1978] concluded that the near-Io sodium cloud is mostly inside Io's orbit, extending forward of the satellite about 70° in orbital longitude. Smyth and McElroy [1977] showed that for ejection velocities of a few km/s, atoms from Io spread about 3.5° of longitude per hour into a torus centered on the satellite's orbit. The cloud's angular extent thus implies a sodium lifetime of about 20 hr at the periphery. However, a much shorter lifetime may apply to most Io-generated sodium, as discussed in Section 6.3. The distribution of the near-Io sodium cloud is shown schematically in Figure 6.2.

Systematic variations other than the Doppler brightness modulation have been observed in the near-Io sodium cloud. Trafton and Macy [1975; Trafton, 1977] reported that the sodium emission to the north or south of Io is strongest on the side away from the Jovian magnetic equator. This effect was also observed by Münch and Bergstralh [1977] and Pilcher and Schempp [1979]. It appears to be caused by an interaction between the atoms and the plasma torus, and electron-impact ionization and ion–atom collisions are candidate processes. Morphological variations [Goldberg et al., 1978, 1981] and second-order brightness variations with Io's orbital longitude

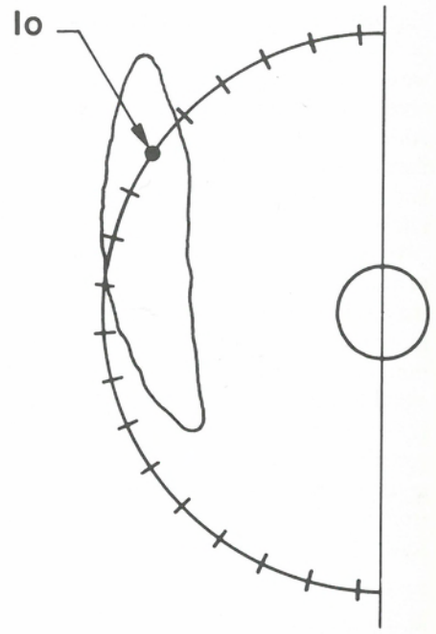

Fig. 6.2. A model of the Io Region B sodium cloud as seen from above Jupiter's north pole [from Smyth and McElroy 1978].

[Bergstralh et al., 1975, 1977] have been attributed by Smyth [1979] to the effects of solar radiation pressure.

There have been many reports of faint sodium emission at great distances from Io [Mekler and Eviatar, 1974; Wehinger and Wyckoff, 1974; Mekler et al., 1976; Wehinger et al., 1976; Trafton and Macy, 1978; Pilcher and Schempp, 1979]. Because of the difficulty in distinguishing this phenomenon from telluric airglow, the nature and even existence of remote sodium had been controversial [Goody and Apt, 1977]. Brown and Schneider [1981] found two distinct kinematical components. The "normal" signature of atoms on bound orbits with large apojoves seems always to be present; these atoms are probably an extension of the bright, near-Io sodium cloud. The signature of "fast" atoms with speeds up to at least 100 km sec^{-1} is seen only occasionally. Brown and Schneider [1981] suggest it is due to sodium produced in the near-Io cloud by collisions between atoms and heavy ions in the corotating plasma. Ion–atom collisions are discussed in Section 6.3.

Other energetic phenomena have been observed in the sodium cloud near Io that may also be caused by ion–atom collisions. Trafton [1975a] and Trafton and Macy [1977, 1978] found asymmetric *D*-line spectral profiles for the near-Io sodium cloud showing velocities as high as 18 km/s with respect to Io. They concluded that sodium is "streaming" away from Io in the direction of its orbital motion. Similar profiles and conclusions were reported by Carlson et al. [1978]. Transient and anomalous directional features in the Io sodium cloud that have been reported in images [Pilcher, 1980b,c; Pilcher and Strobel, 1982], may be collisionally generated streams of sodium.

The brightness of Jovian sodium emission at large distances from Io has been used to infer the plasma electron density under the assumption of depletion by electron-impact ionization [Mekler and Eviatar, 1978, 1980; Goldberg et al., 1981; Eviatar et al., 1981a]. These authors propose that a decrease in distant sodium emission indicates an increase in plasma density. However, this is not necessarily true. The ion and electron densities are locked together by the requirement of charge neutrality; a transient

increase in plasma density would produce both more ionization and more "fast" remote sodium if the Brown and Schneider [1981] mechanism applies. For a fixed Io source rate, the equilibrium production of "fast" remote sodium would be fixed only by the branching ratio for electron-impact ionization and ion–atom elastic collision. It would be independent of the plasma density that would, however, determine the residence time for atoms in the near-Io cloud. The density of distant "normal" sodium, thought to be an extension of this cloud, could therefore be related to the plasma concentration near Io. These considerations suggest that although there is probably a relationship between the plasma density near Io and the brightness of distant sodium, a thorough analysis is necessary before this relationship can be understood. Conclusions [Mekler and Eviatar, 1978, 1980] based on models in which the complexity of the relationship is not taken into account should be viewed with some skepticism.

Resonance emission lines of potassium (7665 A, 7699 A) have also been observed around Io [Trafton 1975b, 1977, 1981]. The distribution of this element seems to be similar to that of sodium. An early suggestion that the potassium lines are more symmetric than those of sodium [Münch et al., 1976] has been superseded by more recent evidence of the kinematic similarities of the two alkali metal clouds (Trauger, private communication, 1981).

Brown [1981a] has reported finding atomic oxygen emission near Io's orbit. His visible detection, $4\pi J$ (6300 A) $= 8 \pm 4$ R is compatible with the upper limit $4\pi J$ (1304 A) < 6.4 R from IUE [Moos and Clarke, 1981]. The spatial distribution of atomic oxygen in the Io torus has not been measured.

The mechanisms by which specific elements are selected and injected from Io into circum-Jovian space have not yet been determined. The ejection speeds implied by the shapes of Io's volcanic plumes are less than the satellite's gravitational escape speed [Cook et al., 1979] and hence inadequate to populate the sodium cloud. Kumar and Hunten [1981] have reviewed sputtering by ion impact, which is possible both at the surface and at the top of the atmosphere [Matson et al., 1974; Haff and Watson, 1979; Haff, Watson, and Yung, 1981]. This mechanism can supply neutral atoms with sufficient speed and also break down low-volatility alkali metals to atomic scale. However, an Io atmosphere poses difficulties for surface sputtering because it may block incoming ions and inhibit the direct escape to space of sputtered atoms [Brown and Yung, 1976]. Furthermore, if atmospheric shielding and surface sputtering are both important on Io, a modulation of the neutral atomic clouds should result from the changing orientation of the corotating ion flux with respect to the highly asymmetrical, solar-fixed distribution of a condensible SO_2 atmosphere [Kumar, 1980]; this effect is not observed [Murcray and Goody, 1978].

Atomic cloud supply rates

The neutral atoms in each region of the Jovian magnetosphere are subject to ionization and so must be replenished constantly. The local sink rates can be estimated from (1) an inventory of atoms based on Equation (6.3), and (2) knowledge of the local lifetime against ionization. Under the reasonable assumption that these atoms originate at Io, the total Io supply rate is the sum of all local sinks. This calculation can be attempted only for the best-studied species, sodium, but a total Io atomic source rate follows from an assumed sodium mixing ratio.

Brown and Schneider [1981] find the "normal" sodium population remote from Io represents a sink $\sim 10^{26}$ atoms/s. The episodic "fast" remote sodium has not been inventoried. These components occupy a region of low plasma density, and the governing loss process is photoionization with lifetime ~ 400 hr [Carlson et al., 1975].

Table 6.2. *Io torus electron density measurements*

Source	n_e(cm^{-3})	Reference
Ground-based [S II] observations	2000[a]	Brown (1976)
Ground-based [S II] observations	3000[a]	Brown (1978)
Voyager 1 ultraviolet spectrometer	≥ 2100	Broadfoot et al. (1979)
Voyager I planetary radio astronomy experiment	2000[b]	Warwick et al. (1979a)
Voyager 1 plasma science experiment	2000[b]	Bagenal et al. (1980)
Ground-based [S II] observations	4000[a,c]	Trafton (1980)
Ground-based [S II] observations	1000[a]	Trauger et al. (1980)
Ground-based [S II] observations	5000[d]	Morgan and Pilcher (1982)
Ground-based [O II] observations	2000	Morgan and Pilcher (1982)

[a] These values have been adjusted by Pilcher and Strobel (1982) from those reported by the individual investigators to remove the effects of differences in assumed collision strengths and electron temperatures.
[b] Variations of a factor of 2 about this value were observed between 5 and 7 R_J.
[c] This value corresponds to the characteristic reported line ratio. Trafton reported large variations about this value.
[d] This value corresponds to the reported mean line ratio; the mean electron density reported by Morgan and Pilcher from the [S II] line observations was $\bar{n}_e = 4000$ cm^{-3}.

Images of the near-Io sodium cloud, but excluding the satellite's immediate vicinity, have yielded both an atom count and a lifetime, as discussed above. Smyth and McElroy [1978] find that a source $\sim 2 \times 10^{35}$ atom/s is required for this region in the absence of a shortened sodium lifetime near Io.

Sodium in the immediate vicinity of Io is difficult to observe because the very high surface brightness of Io's telescopic image reduces contrast [Brown et al., 1975]. Furthermore, the sodium lifetime against electron-impact ionization must be short, so a large atomic sink is probably hidden in this region [Brown, 1981b]. Independent measurements of the Io torus electron temperature and number density are available both from Voyager 1 instruments and from ground-based photometry of forbidden line emission. These results are discussed in Section 6.4 and summarized in Tables 6.2 and 6.3. The major electron component is well characterized by a 4–6 eV temperature and number density $n_e \approx 2000$ cm^{-3}, with a possible small admixture of hotter (100–1000 eV) electrons. Under these conditions, the sodium lifetime is 2–3 hr almost independent of the hot electron component (see Fig. 6.3). We suggest that the remote sodium population and much of the imaged near-Io cloud are atoms that have survived this region of short lifetime. This requires traveling $\sim 0.5\ R_J$ with a radial velocity 1–2 km/s, which requires 5–10 hr and implies an approximate order-of-magnitude loss in the hot, poorly observed region. The total sodium sink is then the same factor times the observed, exterior sinks or $\sim 10^{27}$ sodium atoms/s. Brown and Schneider [1981] have argued that the absence of the kinematical signature of remote sodium produced by electron-capture recombination is consistent with a much larger sodium atom population near Io than heretofore has been observed.

The total Io atomic source can be computed from an estimate of the fractional abundance of sodium. Voyager 1 found ~ 10% sodium ions in the middle magneto-

Table 6.3. *Io torus electron temperature measurements*

	T_e^c		T_e^h			
	10^4K	eV	10^4K	eV	n_e^h/n_e^c	Reference
Voyager 2 ultraviolet spectrometer	6	5	–	–	–	Sandel et. al. (1979)
Voyager 1 ultraviolet spectrometer	10	9	–	–	–	Shemansky (1980a)[a]
Voyager 1 ultraviolet spectrometer	5	4	~120	~100	$2\text{–}5\times10^{-2}$	Strobel and Davis (1980)[a]
Ground-based measurements of [O I] and [S III]	5	4	–	–	–	Brown (1981a)
Voyager 1 plasma science experiment[b]	5.8	5.0	726	626	2×10^{-4}	Scudder et al. (1981)
Voyager 1 ultraviolet spectrometer	8	7	726	626	$\leqslant 1\times10^{-2}$	Shemansky and Smith (1981)

[a] These analyses used less accurate collision strengths.
[b] Values reported for 5.5 R_J.
[c] Superscripts *c* and *h* refer to the cold and hot electron components, respectively.

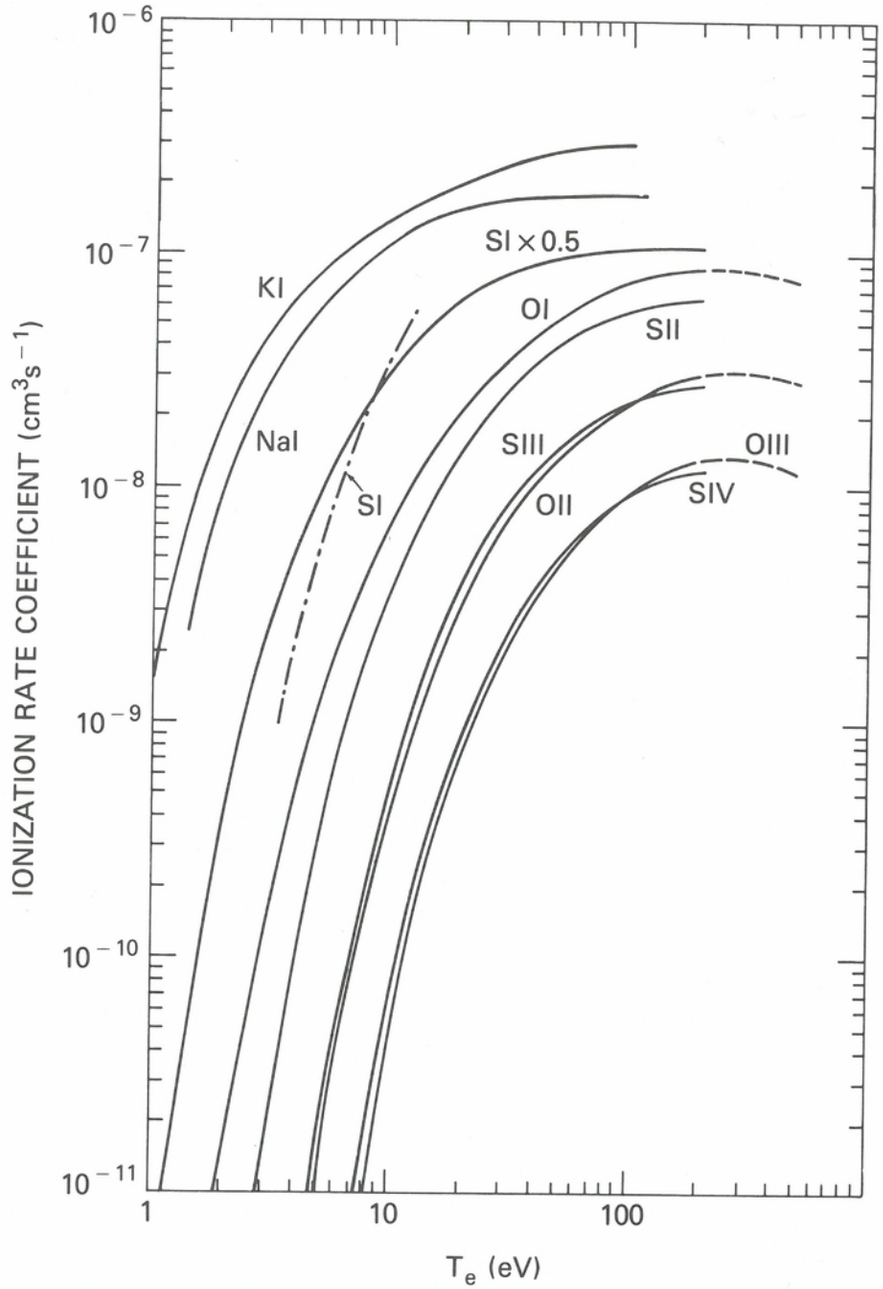

Fig. 6.3. Electron-impact ionization rate coefficients for species present in the Io torus. The coefficients were determined from laboratory cross-section meaurements for O I by Brook et al. [1978], for O II and O III by Aitken and Harrison [1971], and for Na I and K I by Lotz [1967]. The S I coefficients shown by the dash–dot line are based on the theoretical cross sections of Peach [1968, 1971]. All other sulfur coefficients are from the semiempirical expressions of Jacobs et al. [1979]. These tend to be reasonably accurate for ions, but are less accurate for atoms at low temperatures owing to extreme sensitivity to threshold cross-section behavior.

sphere and ~5% in the inner, cool torus (if the gap between the charge-to-mass peaks 16 and 32 is assumed to be filled in by Na^+ [Bagenal and Sullivan, 1981]). If a 5–10% mixing ratio applies to the Io source, the required total atom ejection rate is $\sim (1\text{–}2) \times 10^{28}$ atoms/s. From his determinations of the electron temperature and the neutral oxygen density, Brown [1981a], assuming that electron-impact ionization dominated, concluded that the neutral oxygen ionization rate $d(n_{O\,I})/dt \simeq 2 \times 10^{-4}$ cm^{-3} s^{-1}. If Brown's assumption is correct, neutral oxygen would be expected to form a more nearly complete torus than sodium, centered near Io's orbit [Smyth and McElroy, 1977]. A torus cross-sectional radius of 1 R_J and Brown's value for $d(n_{O\,I})/dt$ leads to a total O I ionization rate of 5×10^{27} s^{-1}. This value is relatively insensitive to the downward revision of the neutral oxygen lifetime when charge exchange is introduced (Section 6.3). The supply rate is proportional to the ratio of the occupied volume and the lifetime, but the former grows proportional to the latter [Smyth and McElroy, 1977]. Ionization rates $\sim 3 \times 10^{28}$ s^{-1} have been estimated from measurements of the total power radiated from the torus, as discussed in Section 6.6.

Ion–atom collisions

Heretofore little consideration has been given to interactions between the corotating heavy ions in the plasma torus and the atoms escaped from Io and forming the neutral atom clouds. In this section we examine elastic and charge exchange collisions, which appear relevant to certain observed torus properties or emission phenomena.

The distribution of encounter speeds for collisions between cloud atoms and plasma ions results from combining the bulk corotational motions with the stochastic distribution of ion velocities in the corotating frame. The former contribution dominates the latter, so we postpone consideration of the ion thermal motions to Section 6.4. At axial distance r from Jupiter, the speed of the corotating ions's cyclotron-guiding center minus the ballistic atom's tangential speed [Brown, 1981a] is

$$v_0(r) = 12.5\, r - (100/r)\ \text{(km/s)} \tag{6.7}$$

which has an average value $\bar{v} \simeq 60$ km s^{-1} in the primary region of plasma/atomic cloud overlap near Io's orbit.

An ion atom collision is described by a cross-section $\sigma(v)$. Practical application requires the rate coefficient,

$$k \simeq \sigma(\bar{v})\,\bar{v}$$

which can be used to compute species' lifetimes and population balances.

Elastic collisions. "Hard" collisions engaging the repulsive core of the interatomic potential will dominate ion–atom elastic reactions when the atom has negligible polarizability. The momentum transfer (diffusion) cross section can be computed from the Thomas–Fermi interaction [see Torrens, 1972]; it is probably a few times 10^{-16} cm^2 for oxygen and sulfur and is a slow function of velocity in the energy range of interest here (Lindhard and Scharff, 1961). The lifetime against such collisions is then:

$$\tau_{TF} = (n\bar{v}\sigma)^{-1} \simeq 100\ \text{hr (sulfur, oxygen)} \tag{6.8}$$

where we have taken $n = 1500$ cm^{-3} as the total ion number density, $\bar{v} = 60$ km/s and $\sigma = 3 \times 10^{-16}$ cm^2.

For an atom of polarizability α, an attractive force results from the dipole moment induced by a passing ionic charge. The momentum transfer cross section for this "soft" interaction [Dalgarno et al., 1958; Dalgarno, 1962] is

$$\sigma_{pol} = 1.0 \times 10^{-14} \frac{Z\alpha^{1/2}}{\mu^{1/2} v} \text{ (cm}^2\text{)}$$

where μ is the reduced mass in amu, Z is the ionic charge, α has units a_0^3, (a_0 = Bohr radius), and v is the encounter speed in km/s. The polarizabilities of Na and K are, respectively, 182 a_0^3 and 257 a_0^3 [Allen, 1973], while those for O and S are about two orders of magnitude smaller. Computation of the lifetime against induced polarization collisions is given by a summation over the various ions with associated charges, reduced mass and number densities = Z_i, μ_i, and n_i:

$$\tau_{pol} = \left[1.0 \times 10^{-9} \alpha^{1/2} \sum \frac{Z_i n_i}{\mu_i^{1/2}} \right]^{-1} \text{ s}$$

independent of ion temperature. For the ion densities from the constant thermal speed model of Bagenal and Sullivan [1981], for example, the induced-polarization collision lifetime would be about 20 hr for sodium and potassium.

The upper limit to the kinetic energy transfer to the atom in an elastic collision is

$$KE_{max} = \frac{4MM_a}{(M + M_a)^2} KE_o$$

where M and M_a are the ion and atom masses, respectively, and KE_0 is the incident kinetic energy. For classical hard spheres, all transfers between zero and KE_{max} are equally probable. In the Thomas–Fermi case, smaller energy transfers are weakly favored because the differential cross section varies approximately as the transferred energy raised to a power between -1 and -1.5 [Lindhard and Scharff, 1961]. Because $KE_0 \simeq (17M)$ eV at Io's orbit (M in amu) and only about 1.5 eV/amu are required for a cloud atom to gravitationally escape the Jupiter system, virtually all hard elastic collisions result in loss from the Io-connected atomic clouds. The soft collisions at larger impact distances will result in much smaller momentum transfers.

The episodic "fast" remote sodium may be produced by hard ion-sodium atom collisions or by charge-exchange (discussed below) [Brown and Schneider, 1981]. The directional sodium cloud features [Pilcher, 1980b,c; Pilcher and Strobel, 1982] may also result from a combination of these processes. The 20 hr lifetime against soft collisions is comparable to the sodium ionization lifetime at the near-Io cloud periphery, which implies the atoms observed in the near-Io cloud have received significant momentum from the plasma ions. This perturbation may be larger than radiation pressure which has been suggested as an explanation of the observed east–west asymmetry [Smyth, 1979]. We believe a reassessment is in order for those conclusions about the Io source magnitude and anisotropy and the launch mechanism which have been based on purely ballistic interpretations of the kinematical and morphological structures of the near-Io sodium cloud.

Charge-exchange collisions. This process has been discussed recently by Cheng [1980], Kunc and Judge [1981], and Brown and Schneider [1981]. The reactions of particular interest are shown in Table 6.4. The cross sections are evaluated for 60 km s^{-1} encounter speed; lifetimes are computed from (6.2), and an assumed 300 cm^{-3} number density for S II and O II and 100 cm^{-3} for the Na II. The combined charge exchange lifetimes of neutral oxygen and sulfur are 80 and 33 hr, respectively, which are competitive with

Table 6.4. *Charge-exchange reactions at 60 km/s encounter speed*

Reaction[a]	$\sigma(E)$ (cm^2)	τ(hr)[c]
$O^+ + O \rightarrow O^* + O^+$	2×10^{-15} [d]	80
$O^+ + S \rightarrow O^* + S^+(^2P^0)$	1.5×10^{-15} [b]	100
$S^+ + S \rightarrow S^* + S^+$	3×10^{-15} [b]	50
$S^+ + O \rightarrow S^* + O^+$	$\leqslant 1 \times 10^{-17}$ [b]	2×10^4
$Na^+ + Na \rightarrow Na^* + Na^+$	1×10^{-14} [e]	50

[a] The asterisk indicates a fast neutral atom. Reactants and products are in the ground term unless otherwise indicated.
[b] Cross section from R. E. Johnson (private communication), evaluated at the average ion–atom encounter energy, about 310 eV for OII and 580 eV for S II.
[c] Atomic lifetime computed from (III-4) using ion number density 3×10^2 cm^{-3} for O II and S II and 1×10^2 for Na II.
[d] Experimental value of Stebbings et al. (1964).
[e] Empirical value using Figure 9 in Hasted (1962).

electron impact ionization of these species. Substantially larger O II and S II number densities are possible (see Sec. 6.4 and Table 6.6), which would significantly reduce the stated charge-exchange lifetimes. The atomic sodium charge-exchange lifetime is longer than the electron-impact lifetime. The speed of the neutral atom resulting from charge exchange always exceeds that required for direct escape from Jupiter's gravity; thus a sizable, perhaps the major, fraction of the torus particles are lost as fast neutrals rather than as radially diffusing ions captured by the solar wind.

The ionization rate of O II is much slower than that of S II (see Fig. 6.3). Thus with the reactions of Table 6.4, preferential conversion of O II to S II occurs with fast O* escape; subsequent ionization of S II would be the net sink since the reaction of S II with O is extremely slow. As a consequence, the sulfur to oxygen ion ratio is enriched relative to what would be expected from SO_2, in agreement with Voyager measurements [Bagenal and Sullivan, 1981; Shemansky and Smith, 1981]. Similarly the atomic S/O ratio should be increased as a result of O* escape. In addition, with O II preferentially converted to S II, the O III/O II density ratio would be significantly less than 1, in agreement with observations discussed in Section 6.4.

Each charge exchange event produces an ion that will subsequently be reaccelerated to corotation. If these events occur frequently enough in comparison to the cooling rate of the ions, only hot ions would occupy the torus. Based on current measurements of the neutral densities, a typical time constant for ion charge transfer is one month, approximately the Coulomb collisional cooling time constant for ions.

6.4. The plasma torus

Two types of ionic emission have been observed from the plasma torus, both of which are excited by collisions with electrons. The forbidden lines at wavelengths between 3000 A and 10,000 A arise from transitions between terms in the p^2 and p^3 ground electron configurations of sulfur and oxygen [Figs. 6.4–6.8]. The more energetic lines are observed only from spacecraft (Pioneer, Voyager, IUE) and are due to allowed transitions that occur at wavelengths ($\lambda < 1800$ A) too short for resonant scattering of sunlight to be an important effect.

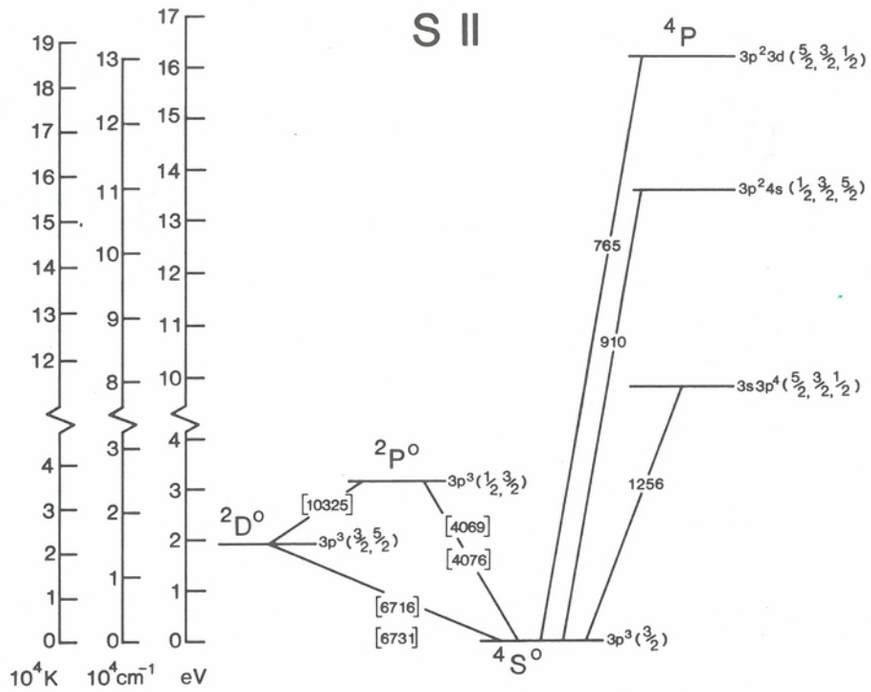

Fig. 6.4. Grotrian diagram for S II. Levels with the same term are shown vertically. The electron configuration and J values (in order of increasing energy) are shown for each level.

The forbidden lines

Optical emission from the torus in the red [S II] lines was discovered by Kupo, Mekler, and Eviatar [1976], and its plasma-diagnostic power was pointed out and first applied to the Jupiter torus by Brown [1976]. The first excited levels of that ion $^2D^\circ_{3/2}$ (1.842 eV), $^2D^\circ_{5/2}$ (1.846 eV), $^2P^\circ_{1/2}$ (3.042 eV), and $^2P^\circ_{3/2}$ (3.047 eV) are connected to the ground state $^4S^\circ_{3/2}$, only by electric quadrupole and magnetic dipole matrix elements (Fig. 6.4). These upper levels are therefore populated only by electron collisions, not by photon absorption. Slow decay by photon emission occurs from the $^2D^\circ_{3/2}$ and $^2D^\circ_{5/2}$ levels with lifetimes 6×10^2 s (6731 A) and 2×10^3 s (6716 A), respectively. The $^2P^\circ_{3/2}$ level radiative lifetime is 1.4 s leading to lines at 4068.6, 10320.5, and 10286.7 A in the ratio 1:0.62:0.51. The $^2P^\circ_{1/2}$ level has a 2.4 s lifetime and yields 4076.4, 10370.5, and 10336.4 A emission in the ratio 1:0.68:1.5 [Osterbrock, 1974]. The differing lifetimes for levels in the same term causes the relative emission rate for lines in a multiplet to depend on the electron density, Eq. (6.6). Collisions will populate the $^2D^\circ$ levels, say, approximately in proportion to their multiplicities, 6 and 4 (neglecting the difference in Boltzmann factor between the $^2D^\circ$ levels and radiative cascades from the $^2P^\circ$ levels). At sufficiently low electron number density, all $^2D^\circ$ ions radiatively decay in the excitation ratio: $[4\pi J\,(6716\text{ A})/4\pi J\,(6731\text{ A})]_{n_e\text{-low}} \simeq 1.5$. At sufficiently high electron number density, collisional deexcitation becomes important. The shorter radiative lifetime of the $^2D^\circ_{3/2}$ level enhances 6731 A emission relative to 6716 A, and the line intensity ratio asymptotically approaches the ratio of the equilibrium populations divided by the corresponding radiative lifetimes: $[4\pi J\,(6716\text{ A})/4\pi J\,(6731\text{ A})]_{n_e\text{-high}} \simeq 0.4$. The transition from one limiting case to the other occurs over that range of electron densities for which the collision time is comparable to the radiative lifetime. At the electron temperatures in the Io torus (Table 6.3), the range is $10^2 < n_e < 10^4\,\text{cm}^{-3}$. The torus electron density is indeed in this range, so $4\pi J$ (6716 A)/$4\pi J$ (6731 A) is a useful indicator of n_e. O II has the same term structure as S II; the corresponding [O II] line ratio, $4\pi J$ (3729 A)/$4\pi J$ (3726 A), is also sensitive to n_e over the same range. Typical electron densities determined from these line ratios are shown in Table 6.2.

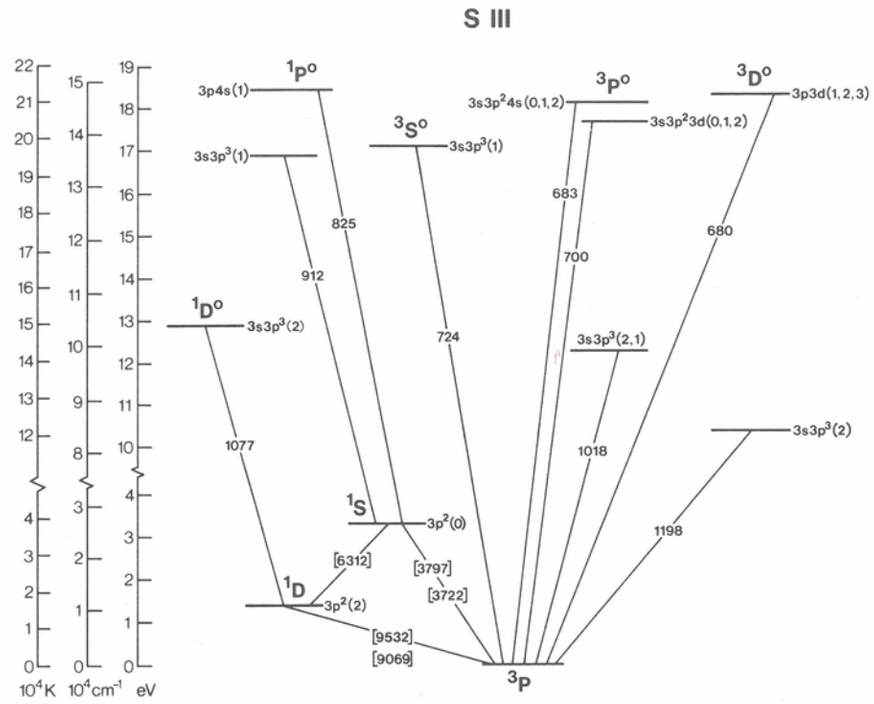

Fig. 6.5. Grotrian diagram for S III.

Because of the much shorter lifetimes, the [S II] ratio $4\pi J$ (4069 A)/$4\pi J$ (4076 A) is sensitive to n_e only for $n_e > 10^5\,\text{cm}^{-3}$, higher density than has been observed in the Io torus. Since the small energy difference between the $^2P^\circ$ levels leads to virtually identical dependences of the rate coefficients of these lines on T_e, this line ratio as observed around Jupiter is essentially independent of the distribution of electron speeds.

The intensity ratio of either blue [S II] line to either red line (for example, $4\pi J$ (4069 A)/$4\pi J$ (6731 A)) is sensitive primarily to T_e for $n_e < 10^4\,\text{cm}^{-3}$, but a dependence on electron number density appears for $n_e > 10^4\,\text{cm}^{-3}$. Morgan and Pilcher [1981] found occasional values of this line ratio not consistent with the electron densities and temperatures of Tables 6.2 and 6.3. These anomalous high blue-to-red emission ratios appear to imply transient high electron density ($n_e > 3 \times 10^4\,\text{cm}^{-3}$) and low electron temperature ($T_e < 1 \times 10^4$ K).

The extreme ultraviolet lines

In addition to the visible and near UV radiation detected by ground-based instruments, the Io plasma torus emits substantial radiation in the extreme ultraviolet (EUV). Weak emission from an incomplete torus was first detected by the Pioneer 10 UV photo-

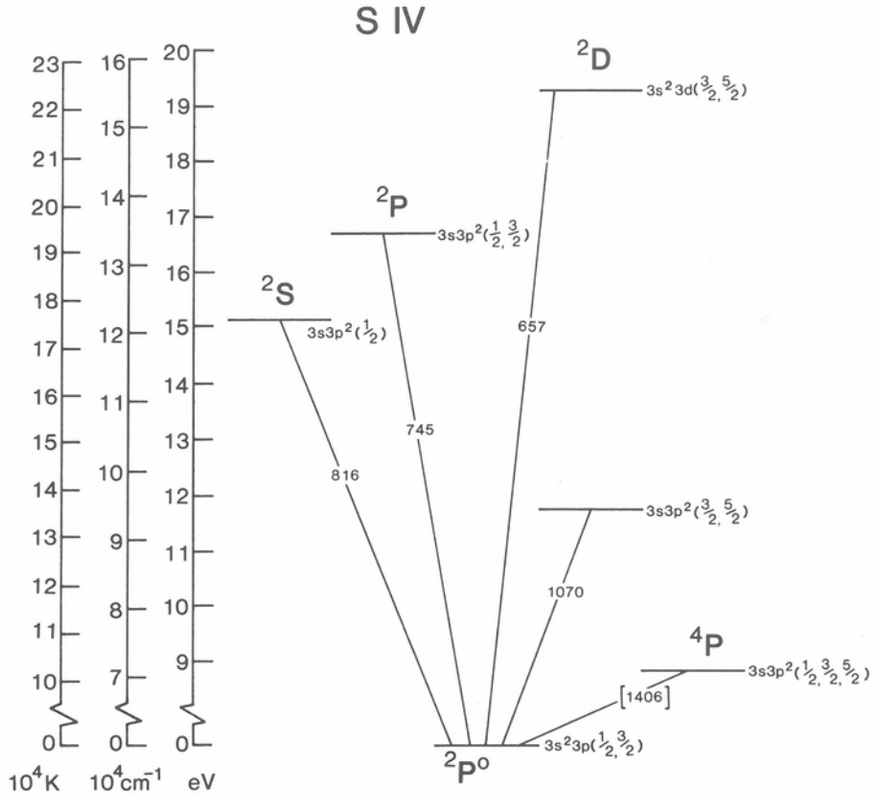

Fig. 6.6. Grotrian diagram for S IV.

meter in both its short (~ 40 *R* for λ < 800 A) and long (~ 300 R for λ < 1600 A) channels [Judge et al., 1976]. The ultraviolet spectrometer (UVS) on Voyager 1 measured strong EUV emission (2–3 × 10^{12} W) from a complete torus [Broadfoot et al., 1979]. The EUV power is about two orders of magnitude greater than the power emitted in the forbidden lines observed from the ground. Observations from rockets and Earth-orbiting telescopes provide continuing ultraviolet measurements [e.g., Moos and Clarke, 1981].

The general characteristics of the Voyager UVS spectra (Fig. 6.9) have been described by Pilcher and Strobel [1982] and can be summarized as follows. The spectra are dominated by features centered at 685 and 833 A. The former is primarily due to overlapping multiplets of S III plus a contribution from O III. The 833 A feature is due to nearly-coincident multiplets of O II and O III plus smaller contributions from S III and S IV. The 685 A feature is surrounded by multiplets of S III (724 A, 729 A) and S IV (657 A, 745 A) that contribute to the wing intensities. There is a persistent feature of S II at 765 A and a variable emission near 910 A that may be due to a blend of an S II multiplet at 910 A with an unknown feature at ~900 A. At longer wavelengths there are multiplets of S III (1018, 1077, 1198 A) and S IV (1070 A). Unlike the forbidden lines observed from the ground, none of these multiplets are resolved in the UVS spectra since the instrument has only 30 A resolution. Thus, the fractional contribution of each multiplet is difficult to determine separately.

Emission from S II has been detected at 1256 A with higher spectral resolution by means of IUE [Moos and Clarke, 1981]. IUE spectra also show emission from S III

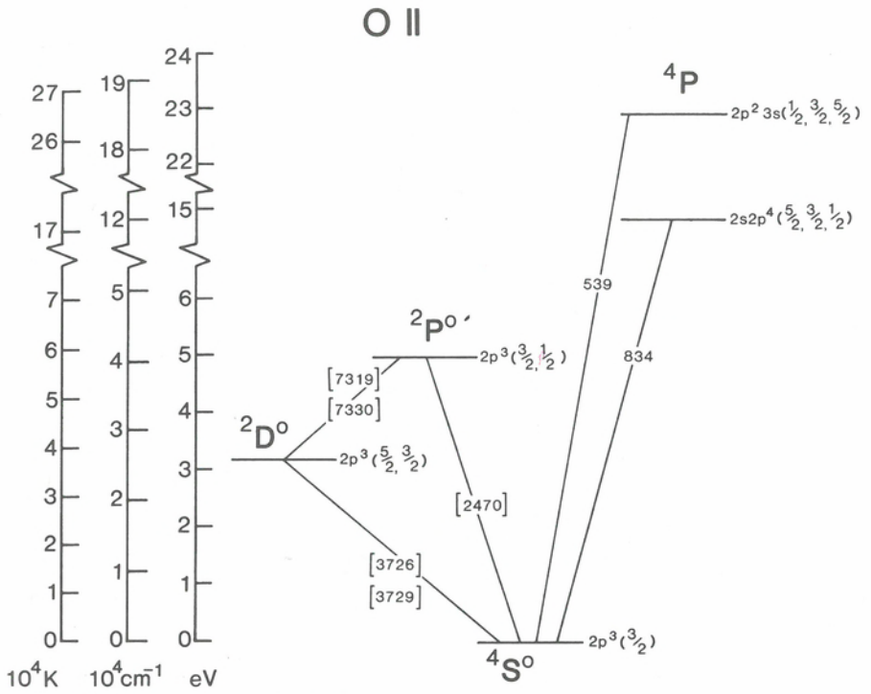

Fig. 6.7. Grotrian diagram for O II.

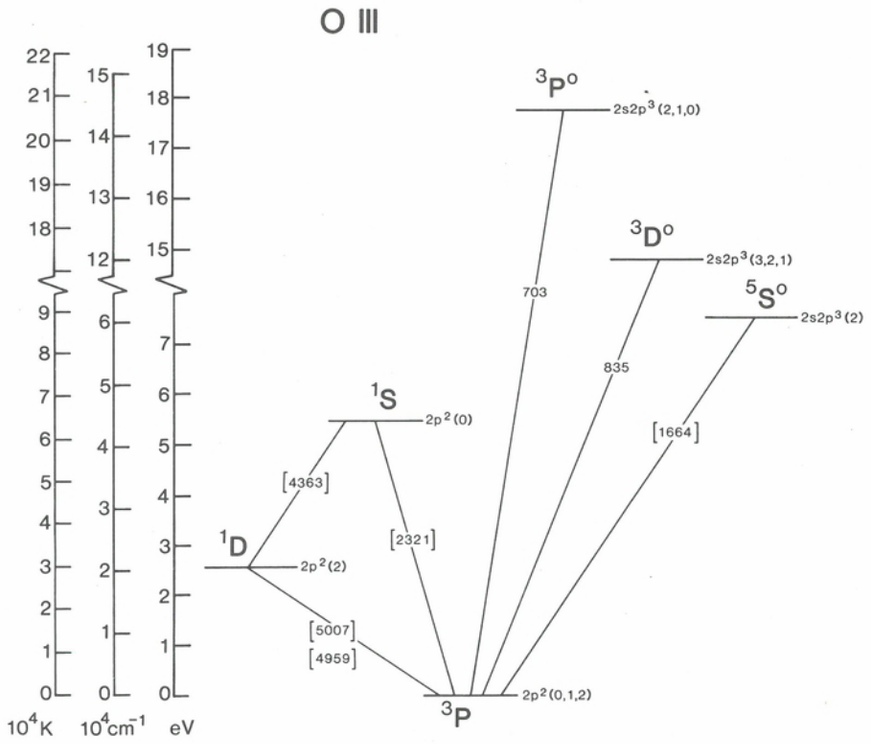

Fig. 6.8. Grotrian diagram for O III.

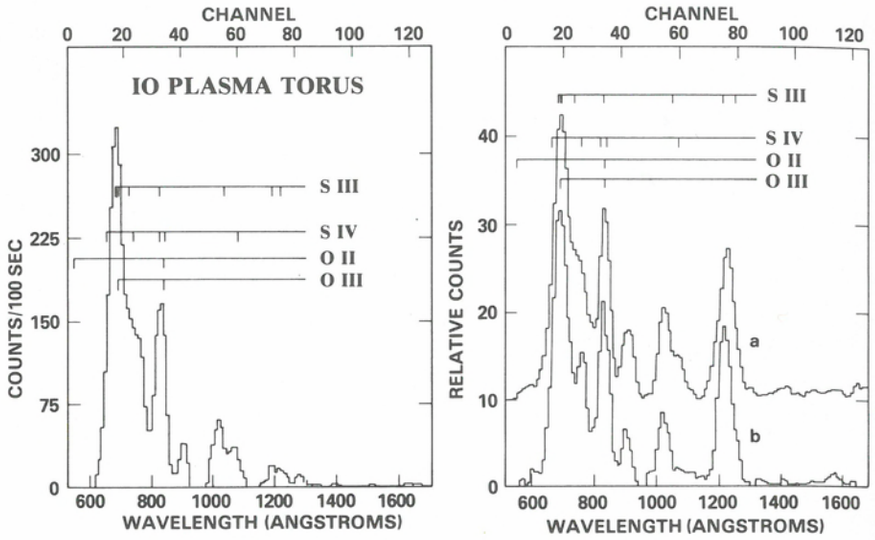

Fig. 6.9. (Left) Voyager 1 EUV spectrum of the plasma torus at elongation; sky background and instrumental scattering have been removed. Multiplets of identified species are indicated. The feature at 685 A is dominated by S III and has a brightness of 200 *R* [from Broadfoot et al., 1979]. (Right) Voyager 2 EUV spectra of the Io plasma torus showing differences in spectral content indicating composition and/or electron temperature changes. The spectra have been corrected for instrumental scattering. A large fraction of the feature near 1200 A arises from interstellar H Ly-α emission at 1216 A. The spectrum labeled "a" has been displaced upward by ten units [from Sandel et al., 1979].

(1198 A) and possible weak emission from O III (1664 A) and S IV (1406 A). Moos and Clarke [1981] have proposed that a feature at 1729 A is an intercombination line of S III [Moos and Clarke, 1981].

The allowed transitions observed in the EUV from Voyager and IUE are the result of excitation by electron–ion collisions and prompt radiative decay. The emission rates are sensitive to the electron density and temperature, but collisional deexcitation is unimportant and the rate coefficient α_λ (Sec. 6.2) is a function only of T_e. The unit emission rate in this case is given by [Osterbrock, 1974]

$$\epsilon_\lambda = n_e \alpha_\lambda(T_e) = n_e \frac{8 \times 10^{-14}}{\omega} \frac{\bar{\Omega}}{T_e^{1/2}} \exp\left(-\frac{\Delta E}{T_e}\right) (R\ \mathrm{cm}^2) \qquad (6.9)$$

where ω is the statistical weight of the ground term, $\bar{\Omega}$ is the thermally averaged collision strength, T_e is in eV, and ΔE is energy of the emitted photon in eV. A group of important collision strengths is given in Table 6.5.

In existing analyses of Voyager UVS spectra it has been assumed that conditions are uniform along the line of sight, and the simplified forms (6.4) and (6.5) have been used in deriving plasma parameters. Synthetic spectra are calculated with various values of the electron temperature and density and the ionic densities n_i until a best fit or a group of best fit spectra is obtained. The uncertainties introduced into these calculations by uncertain atomic parameters have been discussed by Pilcher and Strobel [1981]. As of late 1981, the only spectrum that had been subjected to detailed analysis was the

Table 6.5. *Thermally averaged collision strengths*

Ion	Multiplet	λ(A)	Thermally averaged collision strengths[a] T_e = 5–10eV	100eV
S II	$g3p^3\ ^4S^\circ - 3p^4\ ^4P$	1256	2.2	2.7
	$- 4s\ ^4P$	910	1.6	6.4
	$- 3d\ ^4P$	765	7.25	38
S III	$g3p^2\ ^3P - 3d^3\ ^3D^\circ$	680	29	75
	$- 4s\ ^3P^\circ$	683	6.7[c]	20[c]
	$- 3d\ ^3P^\circ$	700	10[c]	22[c]
	$- 3p^3\ ^3S^\circ$	724	12	21
	$3p^2\ ^1D - 4s\ ^1P^\circ$	729	1.5[b]	2.5[b]
	$3p^2\ ^1S - 4s\ ^1P^\circ$	825	0.5[b]	0.8[b]
	$g3p^2\ ^3P - 3p^3\ ^3P^\circ$	1018	3	4.7
	$- 3p^3\ ^3D^\circ$	1198	4	4.5
S IV	$g3p\ ^2P^\circ - 3d\ ^2D$	657	19	27
	$- 3p^2\ ^2P$	745	16	21
	$- 3p^2\ ^2S$	816	2.2	4.2
	$- 3p^2\ ^2D$	1070	4.5	4.5
	$- 3p^2\ ^4P$	1406	4.5	0.4
O II	$g2p^3\ ^4S^\circ - 3s\ ^4P$	539	0.5	0.9
	$-2p\ ^4P$	834	4.3	8.8
O III	$g2p^2\ ^3P - 2p^3\ ^3P^\circ$	703	6.0	9.9
	$- 2p^3\ ^3D^\circ$	834	7.4	9.9
	$- 2p^3\ ^5S^\circ$	1664	1.1	0.45

[a] Values for S IV from Bhadra and Henry (1980) and Dufton and Kingston (1980). Values for O III (1664 A) from Baluga et al. (1980). Values for S II, S III, O II and O III (except 1664A) from Ho and Henry (1982). S III (729 A and 825 A) values from calculations of Strobel and Davis (1980) with empirical adjustments where experimental oscillator strengths are available. Possibly important resonance effects near threshold included only in calculations for O III (1664 A) and S IV (1406 A).
[b] Accuracy may be less than ±50%.
[c] The sum of these collision strengths is more accurate than their relative values.

Voyager 1 spectrum presented by Broadfoot et al. [1979] and shown in Figure 6.9. The results of the most recent analysis of this spectrum [Shemansky and Smith, 1981] are given in Table 6.6. The electron temperatures derived from the Voyager UVS data are shown in Table 6.3.

The determination of the densities of O II and O III from the UVS data is complicated by the superposition of their primary emissions in the 833 A feature. Shemansky and Smith [1981] dealt with this problem by determining the O III contribution from the intensity of its strong but blended multiplet at 703 A; they then assumed that the remainder of the 833 A feature was due to O II. An alternate approach uses the IUE upper limit to O III (1664 A) and the absence of O II (539 A) in the Voyager spectra.

Table 6.6. *Number density (cm^{-3})*

Ion	UVS[a]	UVS (this paper)	IUE[b]	Plasma science ($6\ R_J$)[c]
O II	50	35–4000[e]		130/1100
O III	340	< 110	110	160
O IV	< 17			
S II	44[d]	120[g]	140	430/470
S III	160		240[f]	430/560
S IV	220		90	27/170
S V	≤ 11			
n_e	>1850			

[a] From Shemansky and Smith (1981). Uncertainty 20%. $T_e = 8 \times 10^4$K (7eV) and a 2 R_J thick homogeneous torus are assumed.
[b] From Moos and Clarke (1981).
[c] From Bagenal and Sullivan (1981). Single values or those preceding a slash from constant temperature models; values following a slash from constant thermal speed models.
[d] The uncertainty in the SII density is ± 50%.
[e] See text.
[f] Brightness variations observed corresponding to a range of 160–320 cm^{-3}.
[g] Brown and Shemansky (1982).

From the O III collision strengths of Baluja et al. [1980] and others listed in Table 6.5, we derive (by means of Equations (6.6) and (6.9)) the following multiplet intensity ratios as a function of T_e:

T_e (eV)	3	6	9	30	100
$\frac{4\pi J(\text{OII, 539 A})}{4\pi J(\text{OII, 834 A})}$	0.0061	0.028	0.058	0.07	0.10
$\frac{4\pi J(\text{OIII, 1664 A})}{4\pi J(\text{OIII, 835 A})}$	2.1	0.52	0.32	0.11	0.05

Around the time of the Voyager 1 encounter, $4\pi J$(OIII, 1664 A) was less than 15 R (Moos, private communication). The Voyager 1 UVS data indicate $4\pi J$(OII, 539 A) < 3 R (Shemansky and Smith, 1981). These values lead to the following intensity upper limits as a function of T_e:

T_e (eV)		3	6	9	30	100
$4\pi J$(OII, 834 A)	<	164 R	36 R	17 R	14 R	10 R
$4\pi J$(OIII, 835 A)	<	7 R	29 R	47 R	135 R	285 R

Thus, the Voyager 1 observed intensity at 833 A of 190 R [Shemansky, 1980a] implies either that the source region is cold ($T_e \lesssim 3$ eV) with O II the principle emitter or hot ($T_e \gtrsim 30$ eV) with O III dominant. For regions where T_e is 3 to 10 eV, the $4\pi J$ (O III, 1664 A) upper limit constrains the O III concentration to $< 110\ cm^{-3}$. Similarly,

the O II concentration must be < 35, 140, and 4400 cm^{-3} for T_e equal to 9, 6, and 3 eV, respectively.

To account for 200 R of 833 A emission when $T_e < 3$ eV, a highly improbable O II density is required which exceeds independent measures of electron density (Table 6.2). If the 833 A feature originates with O III in a region having effective electron temperature ~ 30 eV, the plasma measurements may suggest the emitting region is at the outer edge of the torus (~ 7 R_J). Recent observations have placed an upper limit to $4\pi J$ (O III, 5007 A) $\lesssim 3\ R$ [Brown, Shemansky, and Johnson, 1982]. This corresponds to an O III density upper limit significantly below that derived above, and this implies that the suite of emissions now assigned to O II and/or O III cannot currently be reconciled. The most severe constraints on the O II and O III densities are upper limits to O II (539 A) and O III (5007 A).

There are also problems associated with S IV ultraviolet emission. The Voyager UVS intensities for S IV (745 A) and S IV (1070 A) are 150 R and 100 R, respectively [Shemansky and Smith, 1981]. From IUE the S IV (1406 A) intensity is at most 17 R [Moos and Clarke, 1981], which is consistent with the Voyager upper limit of 50 R. Given the collision strengths in Table 6.5, no single consistent effective electron temperature can be inferred from this data set. However, if it is admitted that the 1070 A feature in the Voyager spectra (see Fig. 6.9) is really a blend of the S III (1077 A) and S IV (1070 A) multiplets as would be expected from the relative intensities of S III (1018 A) and S III (1077 A) multiplets in the solar spectrum, then an effective electron temperature $T_e \sim$ 20–30 eV is consistent with the data and suggests that S IV emission occurs primarily at the outer fringes of the torus (~ 7 R_J) where the electron temperature is high [Scudder et al., 1981].

Brown and Shemansky [1982] have recently reviewed the observed visible and UV spectrum of S II. The S II $3p^2\ 3d^4\ P$ term, misplaced by Moore [1971], has been found by Petterson and Martinson [1982] at 16.2 eV and the corresponding ground state transition multiplet occurs at 765 A. The Voyager UVS spectra display a ~ 60 R emission feature at this position that was previously assigned to K III [Shemansky and Smith, 1981]. Brown and Shemansky [1982] find the S II emissions from the vicinity of Io's orbit at the epoch of Voyager 1 are consistent with $T_e \sim 7$ eV, $n_e \sim 1.6 \times 10^3\ cm^3$ and a S II density ~ 120 cm^{-3}. The corresponding values at the epoch of Voyager 2 are 5 eV, 2.3×10^3 and 170 cm^{-3}. The implications of differential varibility in S II emission brightness at UV versus visible wavelengths have yet to be adequately addressed.

The characteristic electron temperature for S III emission is presumably intermediate between S II and S IV ($5 < T_e < 30$ eV). Unfortunately, attempts to accurately calculate the relative collision strengths of the two S III multiplets at 683 and 700 A (the strongest EUV feature) with state-of-the-art computer codes by Ho and Henry (private communication, 1981) and Davis and Strobel (private communication, 1981) have failed because of the extremely strong configuration mixing. In addition it appears that the S III (1018 A) feature may be contaminated by another emitter, which precludes inference of an accurate electron temperature from the intensity ratio of the 685 and 1018 A features. (See Fig. 6.9.)

We are led by the foregoing discussions of intensity ratios to the view that disjoint regions are addressed by remote spectroscopic studies of the Io plasma torus. The singly ionized species are predominant in low electron temperature regions (< 3 eV), whereas O III and S IV emit primarily in regions where $T_e \sim 30$ eV. This picture is consistent with the ionization energies, ion residence times and the radial variation of electron temperature observed from Voyager. It appears that the Io torus is inhomogeneous along the line of sight and that equivalent homogeneous models have fundamental difficulties in accurately inverting remote measurements in terms of local plasma properties.

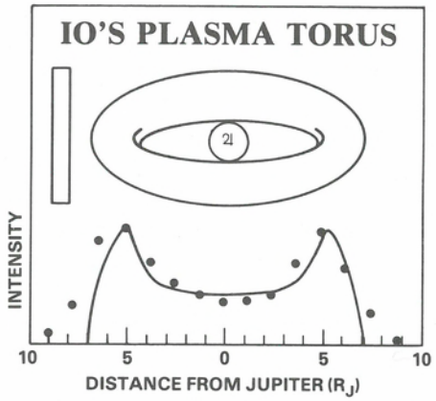

Fig. 6.10. The data points show the measured intensity of the 685 A feature as a function of distance from Jupiter measured in the orbital plane of the satellites. A model torus used to fit the data is shown to scale above the data; the intensity predicted by this model is shown by the solid line. Other observations (not shown) indicate that the intensities at the eastern and western elongation points may differ by as much as a factor of 2 [from Broadfoot et al., 1979].

The EUV emissions observed in 1974 from Pioneer 10 were originally thought to be due in part to atomic hydrogen [Carlson and Judge, 1974; Judge et al., 1976]. If they were in fact primarily due to oxygen and sulfur, then O I (1304 A, 1356 A), O II (834 A), and S II (1256 A) may have been primarily responsible [Mekler and Eviatar, 1980]. The torus seen by Voyager may have been 10 times brighter in the long wavelength channel and 4.5 times brighter in the short wavelength channel of the Pioneer UV photometer than was recorded during the Pioneer encounter, according to a preliminary analysis (Judge, private communication, 1980). At the time of the Pioneer encounter the torus was reported to have an angular extent of ~1/3 of Io's orbit and to be revolving with Io's orbital velocity, implying a neutral composition. This is in sharp contrast to the complete, ionized torus observed by Voyager (see Fig. 6.10). Observations of Jupiter and the interplanetary medium by these UV instruments have been shown to be consistent with measured intensities by Earth orbiting satellites. Thus, we are forced to conclude that certain plasma characteristics of the torus have undergone significant changes in the past few years. The interpretation of Pioneer 10 plasma analyzer results by Intrilligator and Miller [1981] suggests that S III, O II, and O III were present in the torus during the Pioneer encounter at as yet undetermined concentrations. However, Mekler and Eviatar [1980] have interpreted the Pioneer 10 UV observations as originating from a predominantly O II and S II plasma. Further analysis of Pioneer data is clearly required before definitive conclusions on compositional differences between the Pioneer and Voyager encounters can be established. This apparent long-term variability of the plasma torus – reflected to a lesser degree in differences between Voyager 1 and Voyager 2 results [Sandel et al., 1979; cf. Fig. 6.10) – is difficult to reconcile with the observed long-term stability of the neutral sodium cloud, which should respond to changing plasma parameters (see Sec. 6.3).

Ion temperature and spatial distribution

Inside 5.7 R_J, the Voyager 1 plasma experiment [Bridge et al., 1979; Bagenal and Sullivan, 1981] found resolved but overlapping peaks in the positive ion energy-per-charge spectra, which were identified as S II, S III, O II, O III, and SO_2^+. These "cool," inner-torus spectra were consistent with locally-equilibrated plasma ions at temperatures a few eV or less, with the temperature falling sharply with decreasing radial distance from Jupiter, down to ~0.5 eV at 4.9R_J. These findings are consistent with the [S II] line-width analyses of Trauger et al. [1979, 1980], which refer to the same region.

Outside 5.7 R_J, the Voyager 1 plasma experiment recorded broad, unresolved spectra. Temperature analysis required external assumptions about the composition and

thermal state of the plasma, but values in the range 40 to 60 eV were found for extreme models [Bagenal and Sullivan, 1981]. Using optical spectroscopy on this "hot" outer torus, Trauger et al. [1979] found ~30 eV from the [S III] λ9531 A emission width, and Brown [1981a] found ~90 eV from the [S III] λ6312 A emission width at a different epoch. Brown and Ip [1981] have shown that the [S II] 6716 and 6731 A line profiles obtained near Io's orbit have extensive, energetic wings. Brown [1982] found from a detailed line shape analysis that the average S II energy is about 60 eV, whereas a simple interpretation of the line width alone implies 5–10 eV. By comparing the optical line widths, we conclude that outside 5.7 R_J S III is probably hotter than S II, and that more energy may be hidden in possible high-speed tails on the distribution functions of S III and other ions. If the ions occupy the same volume, kinetic thermodynamic equilibrium exists neither within nor between ion species.

The temperatures of the ions are an important factor determining their spatial distributions along the magnetic field lines. At the temperatures of the torus ions, the field-aligned component of the centrifugal force on the ions due to Jupiter's rotation dominates the magnetic mirror force. As a result, the ions have a symmetry plane not at the magnetic equator, but near the centrifugal equator where the centrifugal potential energy of an ion along a field line is a minimum [Hill and Michel, 1976; Cummings et al., 1980]. For a dipolar field this surface is a plane whose tilt relative to the rotational equator is about two-thirds of the tilt of the magnetic equator or, for Jupiter, 7°. The height of an ion above or below the centrifugal equator is a measure of its thermal energy along a field line.

Ground-based observations imply that the spatial distribution of S II inside Io's orbit is generally wedge-shaped, the apex of the wedge lying on or near the centrifugal equator [Hill, Dessler, and Michel, 1974] and about 5 R_J from the center of Jupiter [Nash, 1979; Pilcher, 1980a; Pilcher et al., 1981]. This wedge shape agrees well with the ion distribution expected from the strong radial gradient in the ion temperature determined from Voyager data [Bagenal and Sullivan, 1981]. S II formed near Io's orbit may cool during the slow inward diffusion (see Sec. 6.5), collapsing to the centrifugal equator and forming the wedge. The apex of the wedge as oberved from the ground corresponds to the maximum S II density measured from Voyager [Pilcher, 1980a; Bagenal and Sullivan, 1981].

The strong radial gradient in the ion temperature and temporal variations in the torus structure have led to some confusion as to the isotropy of the ion temperature. Eviatar et al. [1979] presented slit spectra of the red S II lines acquired with the slit perpendicular to the Jovian equatorial plane and 5 R_J from the center of the planet's disk. One of the spectra was acquired when the tilted plasma torus was seen approximately edge-on, thus providing a measure of the thickness of the torus. The parallel temperature of 38 eV derived from this measurement was compared with the perpendicular ion temperature of ~2 eV derived from line width measurements by Trauger et al. [1980]. Because both sets of data were acquired at approximately the same apparent radial separation on the sky from Jupiter, they concluded that the ion temperature exhibits a substantial anisotropy. The line of sight of Eviatar et al. passed through the entire torus, but the results are weighted geometrically toward the emitting region near 5 R_J. They noted that a second spectrum obtained the following night "indicates that the nebula has a fairly large radial extent in addition to its thickness." It seems likely, therefore, that they were looking through the wedge, accounting at least in part for the substantial thickness they measured. The measurements of Trauger et al. were apparently acquired on a night when the wedge was absent, and therefore refer entirely to the cool plasma inside Io's orbit. Subsequent line shape measurements [Brown, 1982] have shown hotter S II at larger distances from Jupiter, consistent with the presence of

a radial ion temperature gradient. We therefore conclude that there is no convincing evidence for ion temperature anisotropy in the plasma torus.

Pilcher et al. [1981] have shown that the structure of the S II component of the plasma torus varies strongly with both magnetic longitude and time. They found the [S II] 6731 A wedge on a particular night (13 UT March 1981) only between magnetic longitudes System III (1965) = 140°–230°. At higher longitudes (up to at least 325°) the S II emission was concentrated near 5.7 R_J, the distance from Jupiter at which both the Voyager plasma science and planetary radio astronomy experiments detected a charge density maximum [Bagenal and Sullivan, 1981]. At lower longitudes (to at least 60°) there was evidence only of the concentration of S II near 5 R_J. This structural variation with magnetic longitude was far less pronounced a month later in April. In the March data, S II emission extended well beyond Io's orbit (out to 7–7.5 R_J) for longitudes between 150° and at least 325°. Other observations showing S II emission beyond Io's orbit and/or intensity variations with magnetic longitude have been presented by Trafton [1980], Trauger et al. [1980], Pilcher and Morgan [1980], Morgan and Pilcher [1982], and Brown and Shemansky [1982].

These variations of S II forbidden line brightness with magnetic longitude must be due to a corresponding variations of electron or S II density or both. In the EUV-emitting torus, where S II is a minor constituent, the electron density appears to be independent of magnetic longitude (Shemansky and Sandel, 1981; Brown and Shemansky, 1982). Longitude-systematic variations in the S II forbidden line brightness near Io's orbit must therefore be due to variations in the S II number density. S II is a dominant component of the plasma well inside Io's orbit, where it comprises as much as half or more of the total charge density (Broadfoot et al., 1979). In this region variations of the forbidden line brightness probably reflect a variation in plasma mass and charge density with magnetic longitude.

Although S II emission is often observed outside of Io's orbit, most of the sulfur at these distances is more highly ionized. The Voyager 1 plasma science experiment found S III was largely absent in the relatively cool plasma inside of 5.5 R_J where S II was abundant. The S III was found to extend to ~7.5 R_J with maximum density at Io's orbit [Bagenal and Sullivan, 1981].

The spatial distribution of S III EUV emission measured from Voyager 1 before encounter is shown in Figure 6.10 [Broadfoot et al., 1979]. The data were fit with the model torus shown in the figure: a radius of symmetry of 5.9 ± 0.3 R_J and a cross-sectional radius of 1.0 ± 0.3 R_J centered on the magnetic equator (although it was not possible to distinguish on the basis of the data between this plane and the centrifugal equator. The intensity distribution corresponding to this model is shown as a solid line superimposed on the data in Figure 6.10. The EUV emission extends beyond the outer boundary of this homogeneous torus, but is consistent with a rather well defined inner edge near 5 R_J.

These data combined show that although there is some spatial separation of S II and S III in the torus, there is a substantial region of overlap. This leads to an inconsistency, as pointed out by Shemansky and Smith [1981]. The S II emission observed from the ground shows a marked variation with longitude and time. The EUV emissions, on the other hand, show no long-term magnetic longitude dependence, only a Jupiter local-time asymmetry, and they are much less temporally variable [Sandel et al., 1979; Shemansky and Sandel, 1981; Sandel and Broadfoot, 1982]. Because S II is presumably the source of S III, the brightness variations of the former are somehow suppressed from manifesting themselves in the emission characteristics of the latter. Shemansky and Smith [1981] have suggested that this suppression might result from a long diffusive loss time. Alternatively, the S II emission may reflect the production rate rather

than the spatial density of the ion. A third possibility is that the longitude-variable S II is decoupled from the EUV-emitting and longitude-invariant S III (Brown and Shemansky, 1982). The UV local time asymmetry is interpreted by Shemansky and Sandel [1981] as a 10 hr periodicity in electron temperature.

Pilcher et al. [1981] have suggested that the S II emission from the hot torus (i.e., outside of Io's orbit) may be the product of plasma that was created at or just inside of Io's orbit and is observed as it streams rapidly outward. Radial velocities of order 1 km sec^{-1} are suggested by the short lifetime of S II in the hot plasma. This apparently rapid plasma transport over a limited range of magnetic longitudes [Pilcher et al., 1981] is qualitatively consistent with the description of corotating magnetospheric convection presented by Hill, Dessler, and Maher [1981]. However, there is no reported evidence of this rapid outward transport in the Voyager EUV data.

A difference between the spatial distributions of ionized sulfur and oxygen has been detected both from Voyager [Bagenal and Sullivan, 1981] and from the ground [Pilcher and Morgan, 1979, 1981]. Oxygen is present at greater distances from the symmetry plane of the torus, an effect that appears to be a result of its smaller mass [Bagenal and Sullivan, 1981].

6.5. Radial transport

Two types of radial transport are present in the Io torus; the ballistic motion of neutrals escaping from Io and the cross-L transport of ions that, at least in part, were formed from these neutrals. Both of these transport mechanisms manifest themselves in spatial distributions of the transported material that are larger than their immediate sources: for example, the radial extent of the neutral sodium cloud is large compared to the diameter of Io; the radial extent of the sulfur and oxygen plasma is large compared to the expected dimensions of the neutral clouds of these elements. The spatial distribution of neutrals has been extensively studied [Murcray and Goody, 1978; Smyth and McElroy, 1978; Goldberg et al., 1978; Pilcher and Schempp, 1979] as a means of elucidating the characteristics of the neutral transport mechanism, that is, the directions and velocities of ballistic ejection from Io (see Sec. 6.3). Similarly, the radial distribution of ions determined from the Voyager plasma science experiment has been analyzed in terms of possible characteristics of the source and the radial transport mechanism. Brown and Ip [1981] have argued that extensive neutral clouds are the major ion source, which would have important consequences for the dynamics and structure of the Io torus.

Flux tube interchange diffusion is the cross-L transport mechanism that has been most extensively considered for the plasma torus. Two types of interchange that have been considered for Jupiter are those driven by fluctuating dynamo electric fields in Jupiter's upper atmosphere that map into the magnetosphere [Brice and McDonough, 1973; Coroniti, 1974] and by centrifugal instability resulting in a rapid decrease in plasma density with increasing L-shell [Ioannidis and Brice, 1971; Richardson and Siscoe, 1981; Siscoe and Summer, 1981]. In the presence of plasma distributed non-uniformly in magnetic longitude, centrifugal instability may lead to corotating convection [Hill et al., 1981; see Chap. 10]. Froidevaux [1980] concluded that both types of interchange were possible, whereas Richardson et al. [1980] concluded that only a time-dependent ion ejection rate could account for the Voyager observations, with the rate of centrifugally driven outward diffusion a factor of 50 greater than the inward diffusion rate. (See Chap. 10 for an alternate view.)

In these analyses it was assumed that the ion source term is zero everywhere except at the L-shell of Io. However, this seems highly improbable since the observed exten-

sive atomic clouds of sodium, potassium, and oxygen (Sec. 6.3), and the likely cloud of neutral sulfur, are expected to correspond to ion sources. Further, the absence of enhanced EUV emission when Io is within the field of view of the Voyager spectrometer suggests that copious ionization of oxygen and sulfur atoms is not taking place in the immediate vicinity of the satellite [Shemansky, 1980b], although ionization by Alfvén's [1954] critical-velocity mechanism may not produce such radiation. Attempts to fit the Voyager data with radially extensive ion sources may therefore lead to conclusions significantly different from those summarized above. Nonetheless, it seems clear that ion radial transport rates of the order-of-magnitude of those deduced in the studies cited above are necessary to account for the observed distribution of ionization states.

6.6. Ionization and recombination

Carlson et al. [1975] showed that electron impact ionization is much more rapid than photoionization in the Io torus even for the low ionization potential of neutral sodium (5.14 eV). Rate coefficients for electron-impact ionization for the principal species in the torus are shown in Figure 6.3. In Section 6.3.C we discussed the importance of charge exchange in the ionization of oxygen and sulfur.

The total ionization rate can be calculated under the assumption that the EUV radiation is powered by the magnetic field sweeping of ions created in an extended neutral cloud [Broadfoot et al., 1979; Brown, 1981a]. The acceleration of newly created ions to the corotational velocity results in ion cyclotron-energies of ~ 280 eV and ~ 550 eV for oxygen and sulfur, respectively. This energy may be transferred to the ambient electrons by means of Coulomb interactions or plasma instabilities, and then back to the ions by collisional electronic excitation leading to the emission of radiation [Brown, 1981a,b]. The observed total emission rate of $\sim 2 \times 10^{12}$ W [Broadfoot et al., 1979; Shemansky, 1980a] implies a total ionization rate (for a sulfur-to-oxygen ratio of 0.5) of $\sim 3 \times 10^{28}$ sec^{-1}. In Section 6.3.B we showed that other considerations lead to an estimate of the total ionization rate in the range $(1\text{–}2) \times 10^{28}$ sec^{-1}. The comparability of these rates implied by the radiated EUV power supports the assumption made above that the original source of the radiated power may be Jupiter's rotation transferred by the acceleration of newly created ions.

Shemansky and Sandel [1981] report a 40% EUV brightness modulation pattern stationary in Jupiter local time and stable for at least a half-year. Sandel and Broadfoot [1982] have reported a secondary brightening associated with Io's position. Brightness variations in the EUV-emitting torus must be caused by changes in electron temperature, since significant fluctuations in plasma mass are ruled out by the absence of a magnetic longitude dependence in both the EUV luminosity [Shemansky and Sandel, 1981] and the [S II] ratio $4\pi J$ (6716 A)/$4\pi J$ (6731 A) at 5.9 R_J [Brown and Shemansky, 1982]. Since EUV emission is the main plasma energy sink, these variations seem to reflect modulation of the energy transfer channel(s), the nature of which remains obscure. The local-time and Io-correlated sources apparently supply $\sim 80\%$ and $\sim 20\%$, respectively, of the EUV radiated power.

In the inner torus ($L < 5.8$) radial transport is probably slow (Richardson et al., 1980; Bagenal et al., 1980; cf. Secs. 6.4, 6.5) and ion-electron recombination may affect the ionization distribution. The principal mechanism for recombination in a high-temperature plasma is dielectronic recombination, a process involving the simulataneous change in quantum states of two electrons. It may be viewed as two steps: first, the radiationless capture of an electron with simultaneous excitation of an already bound electron

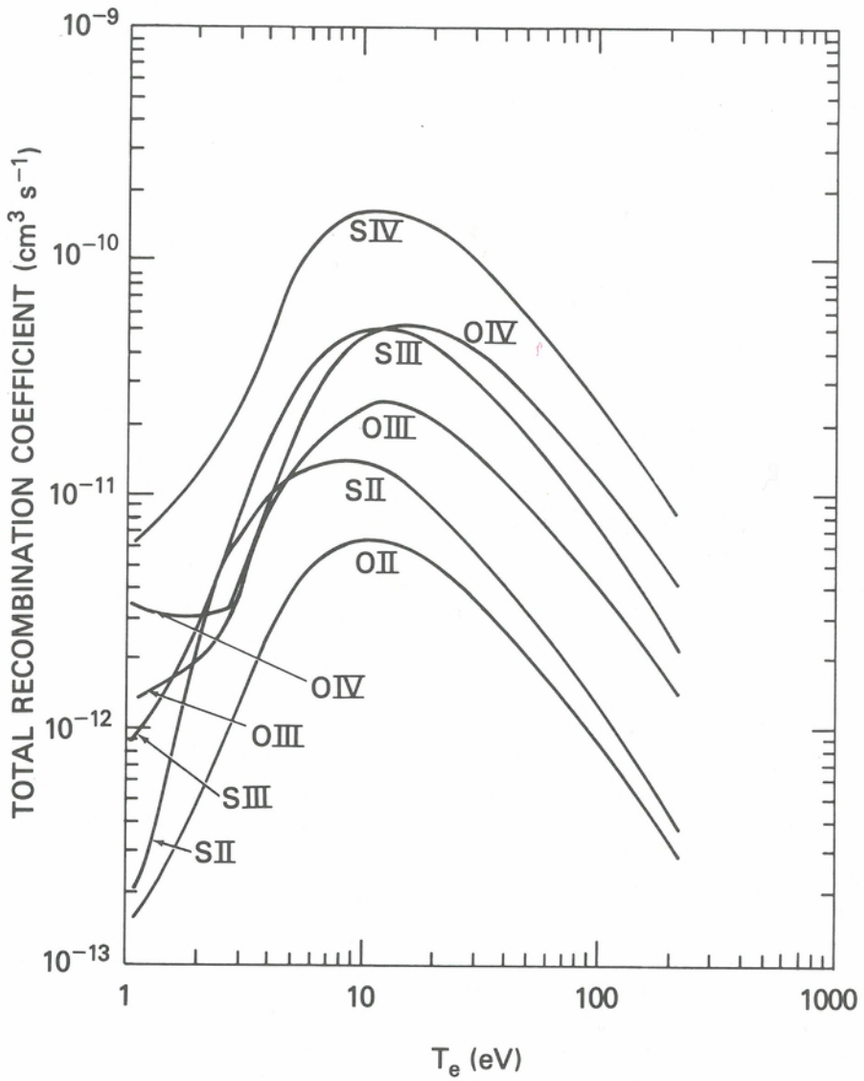

Fig. 6.11. Total (sum of radiative and dielectronic) recombination coefficients [from Jacobs et al. 1978, 1979].

$X^{z+} + e \rightarrow X^{(z-1)+}$ (doubly excited)

followed by a stabilizing radiative transition to a final state below the ionization threshold,

$X^{(z-1)+}$ (doubly excited) $\rightarrow X^{(z-1)+}$ (singly excited) $+ h\nu$

and a subsequent radiative transition. The recombination rate dn_i/dt is given by

$dn_i/dt = \alpha n_i n_e$

where n_i is the density of the recombining ion and α is the total recombination coefficient, including both radiative and dielectronic components. In Figure 6.11 we show α for the principal Io torus ions as a function of T_e. At low electron temperature ($T_e < 1$ eV) radiative recombination dominates, its rate decreasing with increasing T_e. The dielectronic recombination coefficients peak near $T_e \simeq 10$ eV.

6.7. Concluding remarks

Since the discovery of sodium emission by R. A. Brown [1974], our understanding of Jupiter's heavy-ion environment has improved greatly through the union of the Pioneer and Voyager measurements with continuous spectral observations from the vicinity of Earth. A vast and complex geophysical entity has been identified and is now coming into focus. We know Io is the source of a peculiar mix of both neutral and charged material for Jupiter's magnetosphere. Sputtering may be the escape mechanism from Io, but neither this nor any of the details of timing, isotropy, and species selection are established. The relationships between the torus and the active and bizarre properties of Io's solid body are also not known. We believe energy from Jupiter's rotation drives the torus emissions, but adequate models do not yet exist. We see evidence for thermal and convective ion motions and for collisional acceleration of the ballistic neutral atoms, but a coherent picture has yet to emerge of the alternate avenues along which Io-derived particles are transported from source to sink. There is conflicting evidence concerning the torus' temporal variability from Pioneer/Voyager differences and the remarkable stability of the sodium cloud as seen from Earth.

The Io torus studies are contributing to the refinement of theoretical models and diagnostic tools that have direct application to other astrophysical problems. The detection and interpretation of spectral emissions is the classical basis for our view of the physical state and processes that obtain in active galaxies, stellar coronae, and planetary nebulae. The Io torus is by far the most studied and best characterized astrophysical plasma, and it is the first to be intensively observed from near infrared to vacuum ultraviolet wavelengths. Working out the difficult relationship between torus observations at those greatly different photon energies is an activity relevant to interpretations of ultraviolet emission from extra-solar-system objects obtained from Earth orbit.

In this chapter we have summarized first-order physical characteristics of Jupiter's luminous magnetosphere deduced from optical and ultraviolet spectral observations. In concluding, we wish to point out two lines of development that will improve the specificity of future remote studies of the Jupiter plasmasphere. The first is improvement in values of the atomic parameters, such as transition probabilities, collision strengths, and the cross sections for ion/ion and ion/atom reactions, which are vital for modeling emission line observations in terms of intrinsic plasma properties. The second is a better three-dimensional view of the emitting regions. Central to existing analyses has been the simplifying assumption, when one is required, that the emitting region is homogeneous in depth. Variations in radius and longitude are well documented, so this assumption is patently false. In more sophisticated research geometrical factors will be assessed and corrections incorporated into observing techniques and model interpretations. The data base can respond to this requirement: the torus rotates rapidly and so is unfolded in its third dimension by the changing perspective. Through these and other research developments, we expect telescopes to provide continuing and improving observational contact with Jupiter's remarkable plasma environment.

ACKNOWLEDGMENTS

The contribution of R.A.B. was supported by NASA grant NSG-7634. The contribution of C.B.P. was supported by NASA grants NGL 12-001-057, NSG 7403, and NAGW 153. D.F.S. was supported in part by a grant from NASA Office of Planetary Atmospheres; he would like to thank R. J. W. Henry for collision strengths prior to publication, Davis for unpublished collision strength calculations and V. Jacobs for detailed computer output to construct Figs. 6.3 and 6.11.